

Supporting Information

Aerobic selective oxidation of methylaromatics to benzoic acids over Co@N/Co-CNTs with high loading CoN₄ species

*Bingfeng Chen,^a Shaopeng Li,^{abc} Shoujie Liu,^d Minghua Dong,^{ab} Buxing Han,^{abc}
Huizhen Liu^{*abc} and Lirong Zheng^e*

^a Beijing National Laboratory for Molecular Sciences, CAS Key Laboratory of Colloid, Interface and Chemical Thermodynamics, Institute of chemistry, Chinese Academy of Sciences, Beijing, 100190 (P. R. China)

^b School of Chemistry and Chemical Engineering, University of Chinese Academy of Sciences, Beijing, 100049 (P. R. China)

^c Physical Science Laboratory, Huairou National Comprehensive Science Centre, No. 5 Yanqi East Second Street, Beijing, 101400 (P. R. China)

^d College of Chemistry and Materials Science, Anhui Normal University, Wuhu, 241000 (P. R. China)

^e Institute of High Energy Physics, Chinese Academy of Sciences, Beijing, 100049 (P. R. China)

Address correspondence to liuhz@iccas.ac.cn.

Content

Supporting experimental section:

Supporting experimental section including chemicals, catalysts synthesis, catalysts characterization and catalytic reaction.

Supporting Figures:

Figure S1. a) FE-SEM image, b) dark-field TEM image and c, d) HR-TEM images of Co@N/Co-CNTs materials.

Figure S2 a) TEM image, b) bright-field TEM image and c) dark-field TEM image of the Co@N/Co-CNTs materials.

Figure S3. Aberration-corrected HAADF-STEM image of the Co@N/Co-CNTs materials.

Figure S4. XRD patterns of the Co@N/Co-CNTs materials.

Figure S5. N₂ adsorption/desorption isotherm and b) the corresponding BJH pore size distribution curve of Co@N/Co-CNTs.

Figure S6. High-resolution XPS spectra of Co 2p (a) and N 1s (b) in the Co@N/Co-CNTs materials.

Figure S7. a) C K-edge XANES spectra, b) N K-edge XANES spectra, and c) Co L-edge XANES spectra of Co@N/Co-CNTs along with standard MWCNTs and CoPc references.

Figure S8. The XPS survey spectra and Co 2p spectra of Co@N/Co-CNTs sample before and after Ar⁺ sputtering.

Figure S9. Experimental and the fitting k space spectra of Co K edge of Co@N/Co-CNTs.

Figure S10. a) TEM image and b) XRD pattern of the supported Co/N-MWCNTs (Co: 20 wt. %) after reduction at 500 °C for 3.0 h.

Figure S11. a) The influence of molar ratios of cyanamide (CA) to $\text{Co}(\text{acac})_3$ on catalytic properties of Co@N/Co-CNTs ; b) the normalized N species content changes with molar ratios of CA to $\text{Co}(\text{acac})_3$ in Co@N/Co-CNTs .

Figure S12. Raman spectra of the Co@N/Co-CNTs materials synthesized from different mole ratios of cyanamide to $\text{Co}(\text{acac})_3$.

Figure S13. High-resolution XPS spectra of N 1s in the Co@N/Co-CNTs materials prepared by different mole ratios of CA to $\text{Co}(\text{acac})_3$.

Figure S14. DMPO spin-trapping EPR spectrum for Co@N/Co-CNTs in the aerobic oxidation of toluene.

Figure S15 The proposed toluene oxidation mechanism over Co@N/Co-CNTs .

Figure S16 a) The recycle experiment in the toluene oxidation with Co@N/Co-CNTs ; b) the Co 2p XPS spectra of the fresh catalyst and reused for four times.

Fig. 17 HAADF-STEM image of the Co@N/Co-CNTs after cycling.

Supporting Tables:

Table S1 Structural parameters of Co@N/Co-CNTs extracted from the EXAFS fitting.

Table S2. Catalytic performance of several catalysts in the aerobic oxidation of toluene.

Table S3. Catalytic properties of Co@N/Co-CNTs for toluene oxidation with different conditions.

Table S4. The relative concentrations of different N species based on XPS analysis of the several Co@N/Co-CNTs samples.

Table S5. Catalytic oxidation of xylene derivatives with the as-prepared Co@N/Co-CNTs .

Table S6. Comparison of the catalytic performances for selective oxidation of toluene by various catalysts in the absence of radical additives.

1. Experimental section

Chemicals.

Cyanamide, cobalt (III) acetylacetonate ($\text{Co}(\text{acac})_3$), $\text{Co}(\text{NO}_3)_2 \cdot 6\text{H}_2\text{O}$ (98%, trace metal basis), and cobalt (II) phthalocyanine (CoPc) were purchased from Alfa Aesar. Toluene, chlorobenzene, benzaldehyde, benzyl alcohol and benzoic acid were purchased from Sinopharm Chemical Reagent. N-doped multi-walled carbon nanotubes (N-MWCNTs, $\geq 95\%$) was purchased from Aladdin. Tert-Butyl hydroperoxide (TBHP, 70% solution in water), butylated hydroxytoluene (BHT), KSCN, o-xylene, m-xylene, p-xylene, 2-methyl benzaldehyde, 3-methyl benzaldehyde, 4-methyl benzaldehyde, 2-methylbenzyl alcohol, 3-methylbenzyl alcohol, 4-methylbenzyl alcohol, 2-methylbenzoic acid, 3-methylbenzoic acid, and 4-methylbenzoic acid were obtained from Alfa Aesar. Hydrochloric Acid (36.0-38.0%) were purchased from Sinopharm Chemical Reagent Co (China). All of the chemical reagents were analytical grade and used as received without further purification.

Synthesis of Co@N/Co-CNTs materials.

The Co@N/Co-CNTs materials were prepared from thermal-treatment of the mixtures of cyanamide and $\text{Co}(\text{acac})_3$. A certain amount of cyanamide was mixed with $\text{Co}(\text{acac})_3$ in alcohol solution after ultrasonic treatment. The mole ratios of nitrogen compounds and metal precursors changed from 1:4 to 1:12. After removing the alcohol solvent by vacuum evaporation, the mixtures were mixed thoroughly and then transferred into the tube furnace. The heat-treatment was performed under an argon atmosphere at 350 °C (heating rate: 2.5 °C/min) for 3 h, then 650 °C for 3 h and 750 °C for 2 h. The cobalt nanoparticles were removed by acid leaching with 2 mol/L HCl overnight. The as-prepared catalytic material was denoted as Co@N/Co-CNTs.

Preparation of Co/N-MWCNTs catalyst.

The Co/N-MWCNTs catalyst was prepared by the impregnation method using the commercial N-MWCNTs as support. $\text{Co}(\text{NO}_3)_2 \cdot 6\text{H}_2\text{O}$ (0.617 g) was dissolved in 15 mL H_2O , then the commercial N-MWCNTs (0.5 g) was added to the mixture and stirred overnight. After evaporation under vacuum, the solid obtained was dried in vacuum at 80 °C for 24 h. The Co/N-MWCNTs catalyst was activated at 500 °C for 3.0 h under flowing diluted H_2 ($\text{H}_2/\text{Ar}=10/90$ v/v, 50 ml/min).

Catalyst Testing.

Catalytic oxidation was performed in a 12 mL stainless autoclave equipped with a pressure gauge,

a magnetic stirrer, and an electric temperature controller. In a typical run, the catalyst (37.5 mg), and toluene (1.5 mL) were introduced into the autoclave. The autoclave was sealed and purged with O₂ three times. The catalytic oxidation was performed at given temperature and oxygen pressure under stirring. At the end of the reaction, the autoclave was cooled to ambient temperature and slowly depressurized. The catalyst was separated by simple filtration. A known amount of internal standard chlorobenzene was then added to the reactor if used. The quantitative analysis of the reaction mixture was conducted using a GC (Agilent 6820) equipped with a flame ionization detector (FID) and a HP-INNOWAX capillary column (0.25 mm in diameter, 30 m in length). Identification of the products and reactant was done using a GC-MS (Agilent 5977A) with a capillary column (HP-5MS, 30 m, 0.25 mm ID) as well as by comparing the retention times to the respective standards in GC traces.

Characterization.

Powder X-ray diffraction (XRD) patterns were measured on a Rigaku Rota flex diffractometer equipped with a rotating anode and a Cu-K α radiation source (40 kV, 200 mA; $\lambda=1.54056 \text{ \AA}$). FE-SEM images were obtained with SU-8020 (HITACHI) field-emission scanning electron microscope. TEM images were acquired by using JEM-2100F microscope with a beam voltage of 200 kV. Aberration-corrected high-angle dark-field scanning TEM (HADDF-STEM) images were obtained with JEM ARM200F (JEOL) microscope. X-ray photoelectron spectroscopy (XPS) data were recorded on an ESCALab220i-XL instrument with a monochromatized Al-K α line source (300 W) and the peak positions were referenced internally to the C 1s peak at 284.6 eV. To obtain the depth profile of the Co/NCNTs, an Ar⁺ beam (E=1 keV) was used to etch the samples at a rate of 0.05 nm/s (referring to the Ta₂O₅). XPS measurement was conducted after etching for 2.5 min. Nitrogen adsorption measurements were conducted at 77 K on a Quantachrome Quadrasorb SI-MP porosimeter. All samples were degassed at 350 °C for at least 4 h before every measurement. Specific surface areas were determined by the Brunauer-Emmet-Teller (BET) method based on the relative pressure between 0.05 and 0.30. The pore size distribution was analyzed from adsorption branch isotherms by Barrett-Joyner-Halenda (BJH) method. Raman spectra were recorded on a LabRAM HR Raman microscope equipped with 532 nm laser source and 100 \times objective lens. The sample powders were sandwiched with two glass slides before the test. The elemental analysis was performed using a Perkin Elmer Optima 2000 OV inductively coupled plasma-optical emission

spectroscopy (ICP-OES).

EPR spectroscopy was carried out on a JES-FA200 ESR Spectrometer at the X-band at room temperature, with a field modulation of 100 kHz. The microwave frequency was kept at 9.033 GHz. After reaction for 12 h, the spin-trapping reagent DMPO was added to the reaction mixture, and measured in a glass capillary tube by EPR spectroscopy at room temperature.

The X-ray absorption spectra (XAS) including X-ray absorption near-edge structure (XANES) and extended X-ray absorption fine structure (EXAFS) of the samples at Co K-edge were collected at 1W1B station in Beijing Synchrotron Radiation Facility (BSRF), China. A water-cooled Si (111) double-crystal monochromator (DCM) was utilized to monochromatize the X-ray beam and the detuning was done by 10% to remove harmonics. The electron storage ring of BSRF was operated at 2.5 GeV with a maximum current of 250 mA. The EXAFS data of Co K-edge was obtained in the energy range from -200 to 800 eV in transmission mode. The EXAFS oscillations were then extracted according to standard procedures via the ATHENA module implemented in the IFEFFIT software packages. With a Fourier transform k-space range of 0-14.0 Å⁻¹, the quantitative curve-fittings were conducted in the R space according to the module ARTEMIS of IFEFFIT software packages. The phase shift $\Phi(k)$ and backscattering amplitude $F(k)$ were calculated by FEFF 8.0 code. The soft XANES spectra at C K-edge, N K-edge and Co L-edge were measured in TEY mode at beamline 4B7B of BSRF.

2. Supporting figures and tables

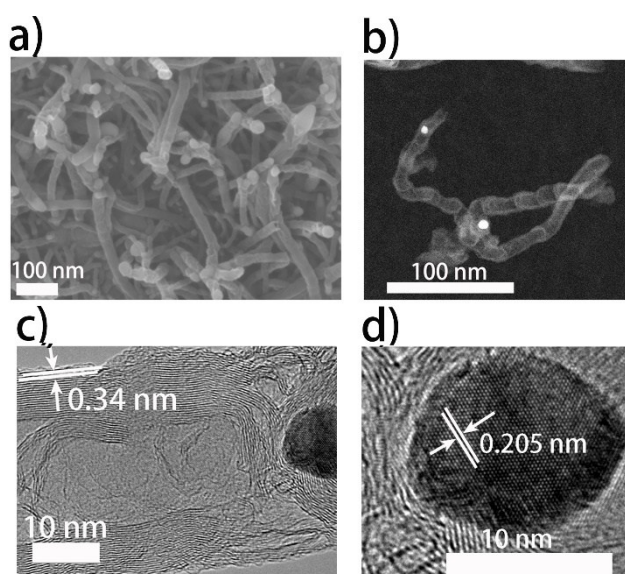


Fig. S1 a) FE-SEM image, b) dark-field TEM image and c, d) HR-TEM images of Co@N/Co-CNTs materials.

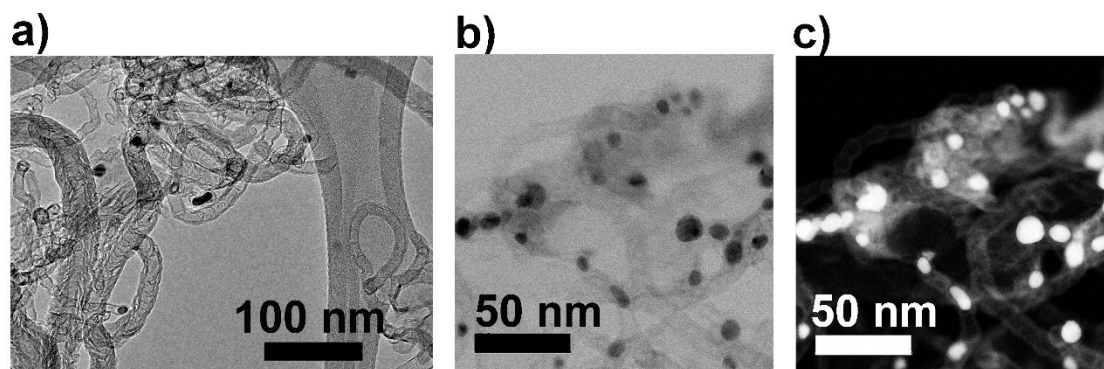


Fig. S2 a) TEM image, b) bright-field TEM image and c) dark-field TEM image of the Co@N/Co-CNTs materials.

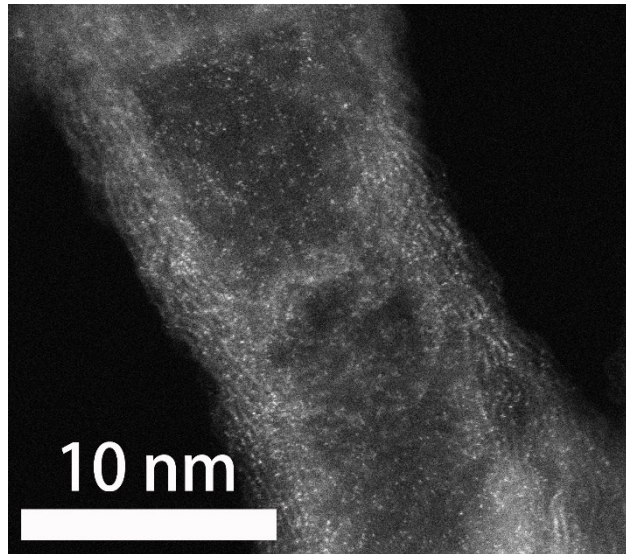


Fig. S3 Aberration-corrected HAADF-STEM image of the Co@N/Co-CNTs materials.

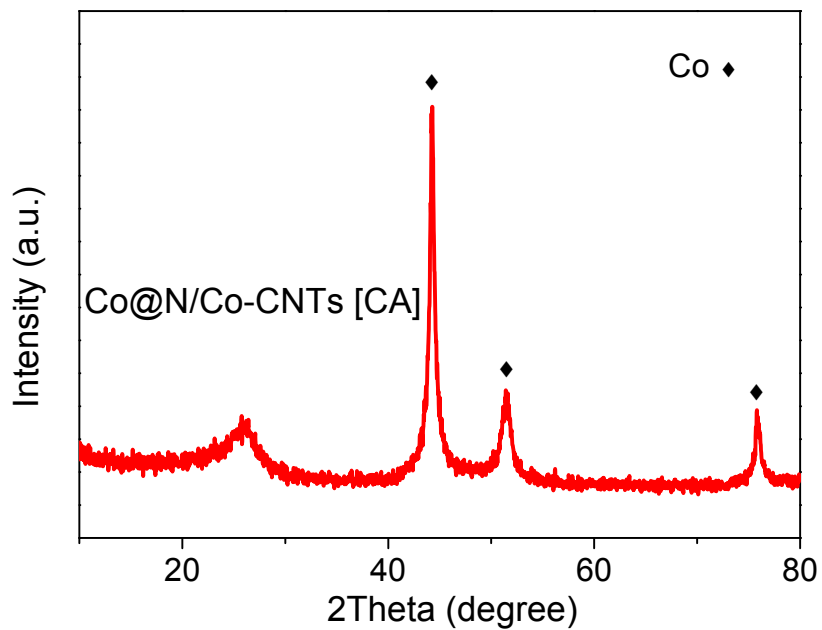


Fig. S4 XRD patterns of the Co@N/Co-CNTs materials.

As shown in Fig. S3, the Co@N/Co-CNTs displayed the main diffraction lines of Co (111), (200), and (220), which were located at 44.2° , 51.5° and 75.8° , respectively. The material also showed a broad peak in the range of $20\sim 30^\circ$, indicating that a carbon framework with partial graphitization was formed.

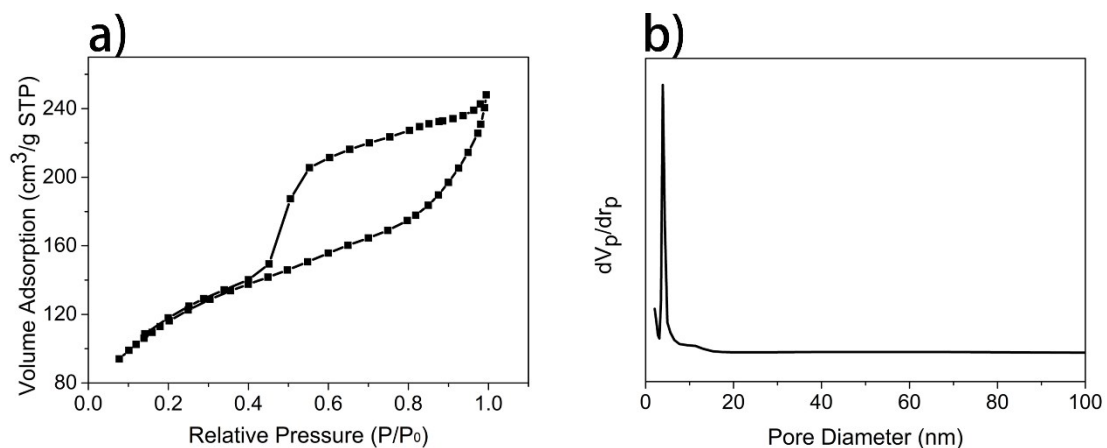


Fig. S5 a) N₂ adsorption/desorption isotherm and b) the corresponding BJH pore size distribution curve of Co@N/Co-CNTs.

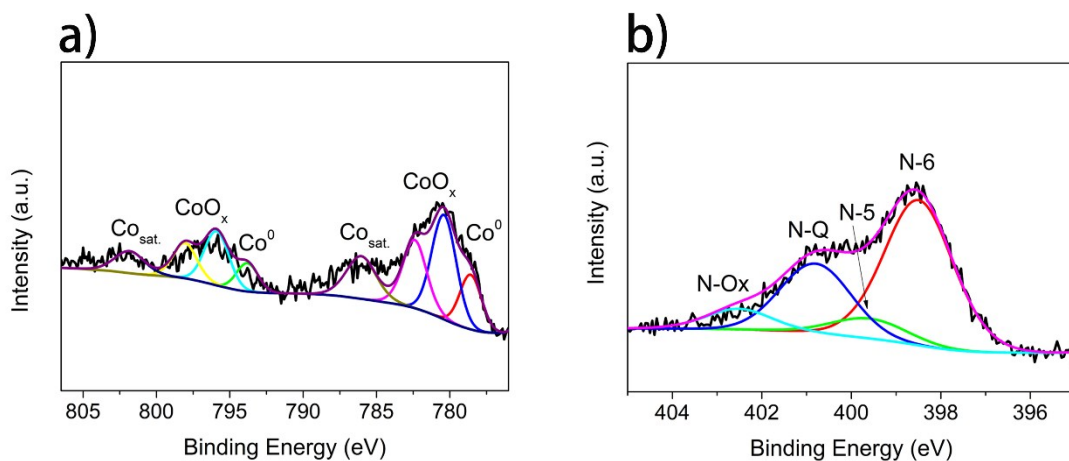


Fig. S6 High-resolution XPS spectra of Co 2p (a) and N 1s (b) in the Co@N/Co-CNTs materials.

As shown in the Co 2p spectrum (Fig. S5a), the peaks around 778 and 793 eV were attributed to Co⁰ specie, while two peaks located around 780 and 782 eV were assigned to cobalt oxidation state (Co^{δ+}).^[1]

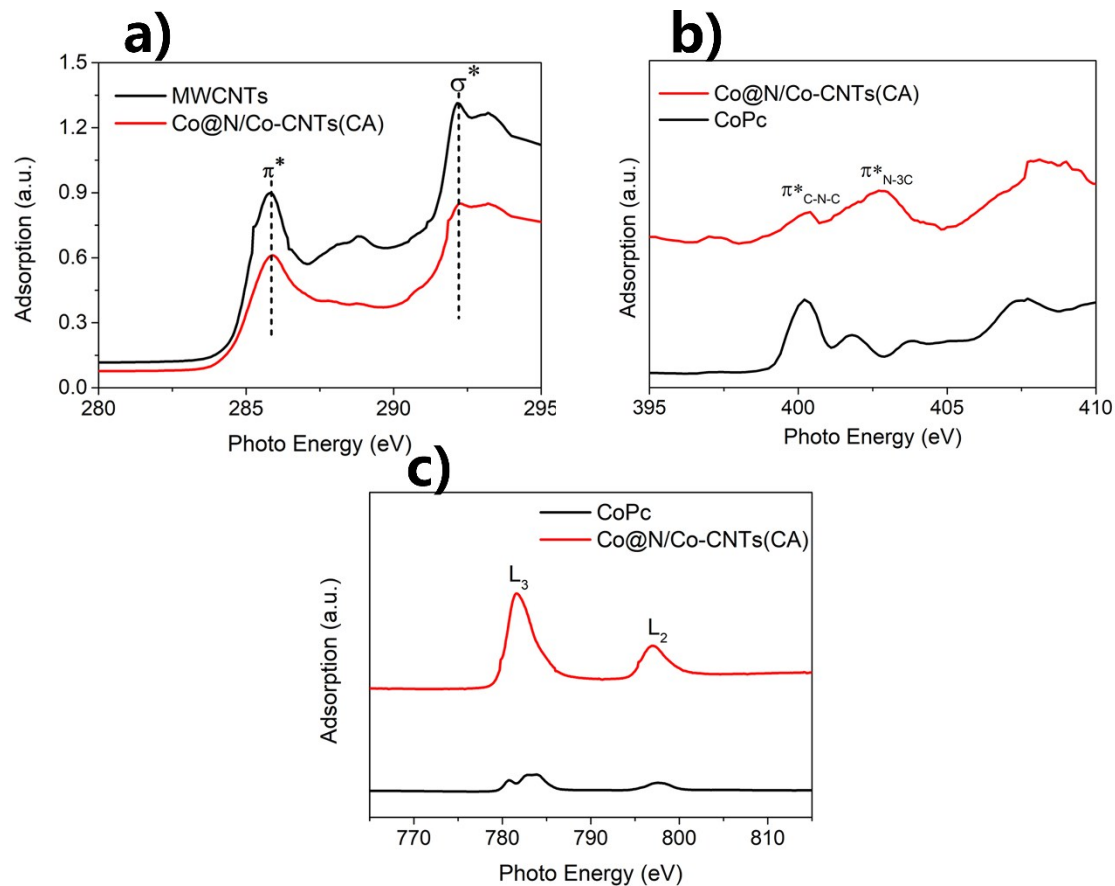


Fig. S7 a) C K-edge XANES spectra, b) N K-edge XANES spectra, and c) Co L-edge XANES spectra of Co@N/Co-CNTs along with standard MWCNTs and CoPc references.

In order to investigate the valence state and electronic structure in the as-prepared materials, soft X-ray absorption near-edge structure (XANES) analysis was conducted. As shown in the C K-edge XANES spectra (Fig. S6a), two feature peaks at ~ 285.5 eV and 292 eV were detected. The former is attributed to the π^* excitation of C=C bonds in a carbon ring, and the latter is assigned to the σ^* excitation of C-C bonds which is sensitive to the long-range order.^[2] The weak adsorption at around 288 eV is ascribed to carbon atoms that are attached to either oxygen atoms or nitrogen atoms.^[3] In the N K-edge spectra (Fig. S6b), the detected peaks located at 400.3 eV and 402.7 eV in the Co@N/Co-CNTs are assigned to the aromatic C-N-C coordination in one triazine heteroring (known as pyridinic, $\pi^*_{\text{C-N-C}}$) and the graphitic bridging among N and C moieties ($\pi^*_{\text{N-3C}}$).^[4] The Co-N (400.2 eV) observed in the cobalt (II) phthalocyanine was overlapped with $\pi^*_{\text{C-N-C}}$ in the hybrid, suggesting the presence of Co-N bonds in the Co@N/Co-CNTs. The Co-L edge absorption (Fig. S6c) of the Co@N/Co-CNTs split into two peaks due to core-level spin-orbit coupling, i.e., the lower energy L_3 peak ($2p^{3/2} \rightarrow 3d$) and higher energy L_2 peak ($2p^{1/2} \rightarrow 3d$).^[5] The Co@N/Co-CNTs showed enhanced absorption in the high energy region compared with that of cobalt (II) phthalocyanine, indicating that the presence of high valence of cobalt (III) in the hybrid material.^[6] This result is consistent with the deconvoluted results of XPS analysis.

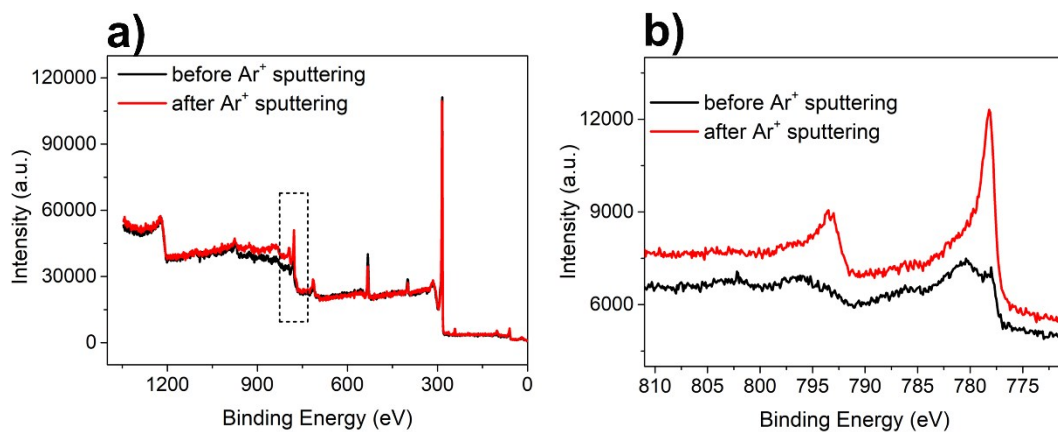


Fig. S8 The XPS survey spectra and Co 2p spectra of Co@N/Co-CNTs sample before and after Ar⁺ sputtering.

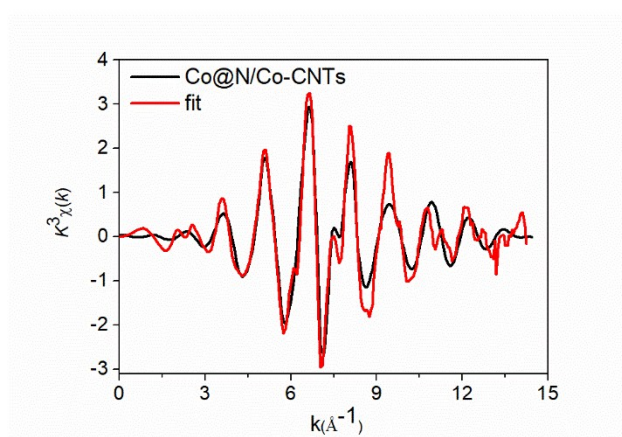


Fig. S9 Experimental (black) and the fitting (red) k space spectra of Co K edge of Co@N/Co-CNTs.

Table S1 Structural parameters of Co@N/Co-CNTs extracted from the EXAFS fitting.
($S_0^2=0.85$)^a

Sample	Scattering pair	CN ^b	R(Å) ^c	$\sigma^2(10^{-3}\text{Å}^2)$ ^d	$\Delta E_0(\text{eV})$ ^e	P ^f
Co@N/Co-CNTs	Co-N	3.8	1.91	9.0	5.2	0.24
	Co-Co	5.9	2.54	7.9		
CoPc	Co-N	4.0	1.90	6.6	5.0	-

a) S_0^2 is the amplitude reduction factor; b) CN is the coordination number; c) R is the interatomic distance (the bond length between central atoms and surrounding coordination atoms); d) σ^2 is Debye-Waller factor (a measure of thermal and static disorder in absorber-scattered distances); e) ΔE_0 is edge-energy shift (the difference between the zero kinetic energy value of the sample and that of the theoretical model); f) p is the fraction of Co single atoms in the sample.

Table S2. Catalytic performance of several catalysts in the aerobic oxidation of toluene. ^a

Ent.	Cat.	Con. (%) ^b	Sel. (%) ^b			Yield BAC (%)
			BAD	BAL	BAC	
1	blank	NR	-	-	-	-
2 ^c	N-MWCNTs	0.2	>99	-	-	-
3 ^d	Co (20 wt. %)/ N-MWCNTs	0.3	>99	-	-	-
4	CoPc	1.1	68.4	-	31.6	0.3
5	Co@N/Co-CNTs	28.0	9.8	0.2	90.0	25.2
6 ^e	Co@N/Co-CNTs	0.4	80.4	19.6	-	-
7 ^f	Co@N/Co-CNTs	1.0	78.4	21.6	-	-

a) Reaction conditions: toluene (1.5 mL), catalyst (37.5 mg), O₂ (3 MPa), 140 °C/15 h; b) The conversions and selectivities were obtained by GC analysis using chlorobenzene as internal standard. BAD: Benzaldehyde, BAL: Benzyl alcohol, BAC: Benzoic acid; c) The commercial N-doped multi-walled carbon nanotubes (N-MWCNTs) was used as catalyst; d) Co (20 wt. %)/N-MWCNTs was prepared by impregnating Co(NO₃)₂ on the N-MWCNTs; e) Additive: KSCN 249.2 mg (Co: 14.8 eq); f) Butylated hydroxytoluene (BHT): 0.15 g.

Table S3. Catalytic properties of Co@N/Co-CNTs for toluene oxidation with different conditions.

Ent.	T (°C) /t (h)	O ₂ (MPa)	Con. (%) ^b	Sel. (%) ^b		
				BAD	BAL	BAC
1	100 / 15	3	0.1	>99	-	-
2 ^c	120 / 15	3	0.2	>99	-	-
3 ^d	140 / 15	3	28.0	9.8	0.2	90.0
4	140 / 15	1.5	0.3	75.9	-	24.1
5	160 / 15	1.5	7.6	28.3	7.7	64.0

a) Reaction conditions: toluene (1.5 mL), catalyst (37.5 mg); b) The conversions and selectivities were obtained by GC analysis using chlorobenzene as internal standard. BAD: Benzaldehyde, BAL: Benzyl alcohol, BAC: Benzoic acid.

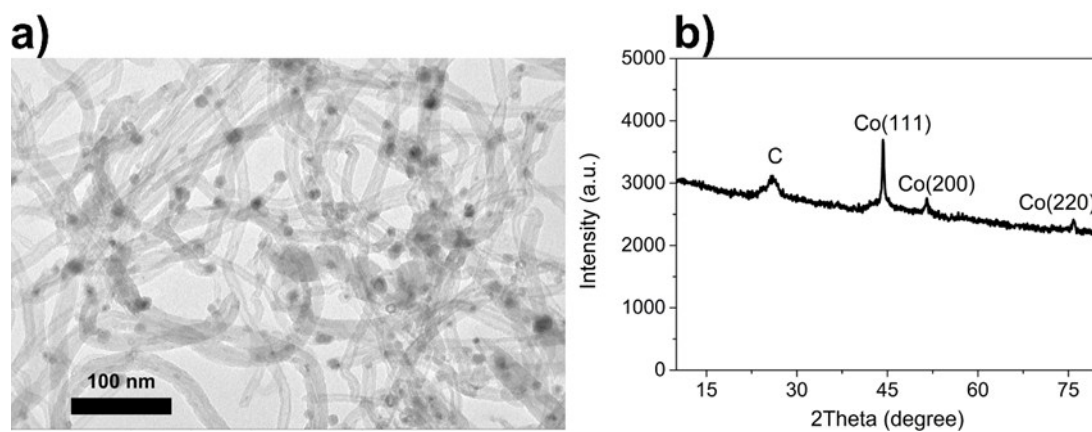


Fig. S10 a) TEM image and b) XRD pattern of the supported Co/N-MWCNTs (Co: 20 wt. %) after reduction at 500 °C for 3.0 h.

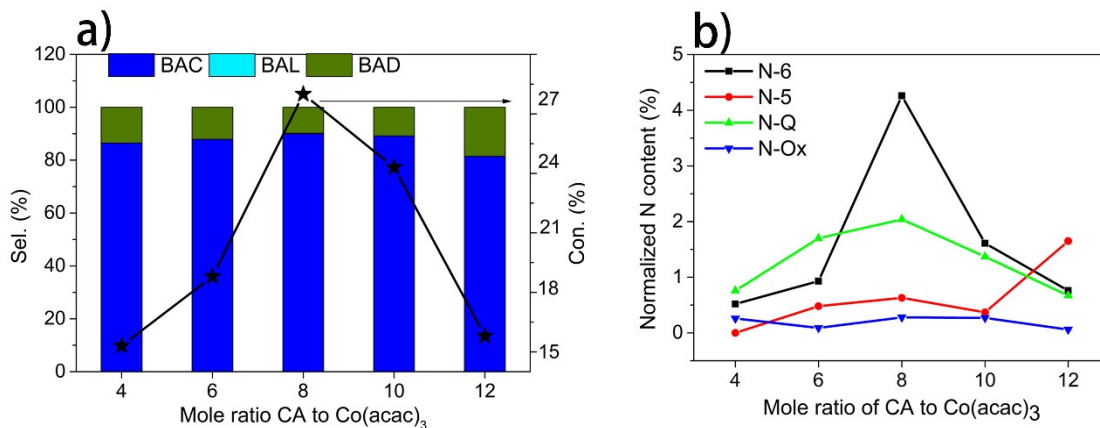


Fig. S11 a) The influence of molar ratios of cyanamide (CA) to Co(acac)₃ on catalytic properties of Co@N/Co-CNTs; b) the normalized N species content changes with molar ratios of CA to Co(acac)₃ in Co@N/Co-CNTs. Reaction conditions: toluene 1.5 mL, catalyst 37.5 mg, O₂ 3 MPa, 140 °C/15 h.

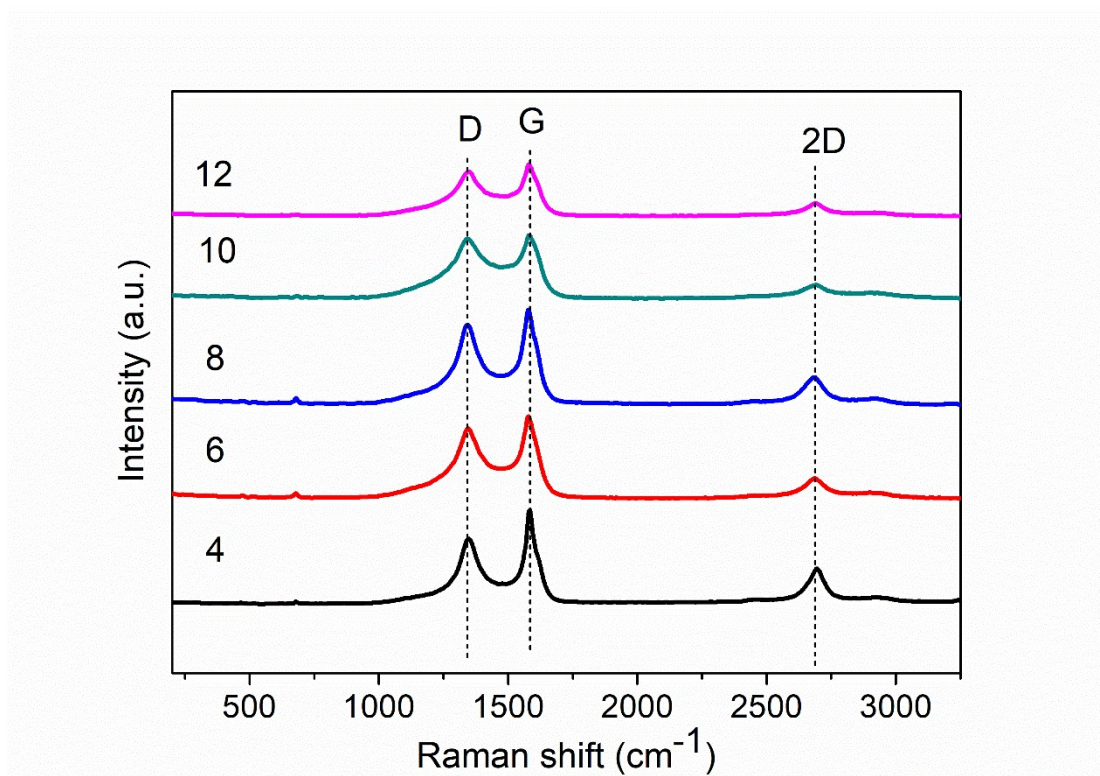


Fig. S12 Raman spectra of the Co@N/Co-CNTs materials synthesized from different mole ratios of cyanamide to Co(acac)₃.

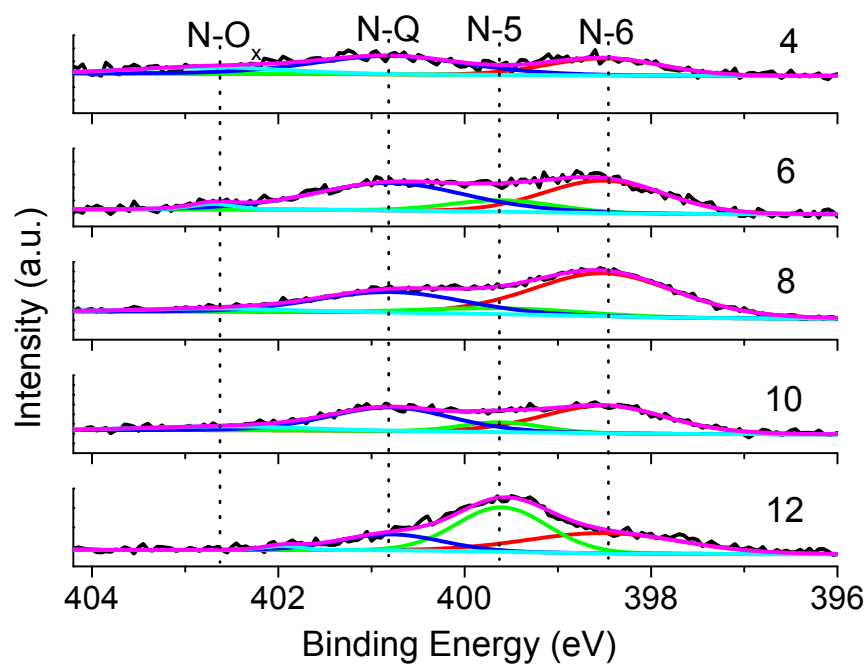


Fig. S13 High-resolution XPS spectra of N 1s in the Co@N/Co-CNTs materials prepared by different mole ratios of CA to Co(acac)₃.

Table S4. The relative concentrations of different N species based on XPS analysis of the several Co@N/Co-CNTs samples

Catalyst	Co (atom %)	C (atom %)	O (atom %)	Total N (atom %)	Relative concentration of different N species (area %)			
					N-6	N-5	N-Q	N-O _x
Co@N/Co-CNTs (CA: Co(acac) ₃ =4) ^a	0.91	95.48	2.07	1.54	33.8	0	49.2	17.0
Co@N/Co-CNTs (CA: Co(acac) ₃ =6) ^a	1.16	90.81	4.84	3.20	29.0	15.1	53.1	2.8
Co@N/Co-CNTs (CA: Co(acac) ₃ =8) ^a	1.79	83.89	7.1	7.22	59.1	8.7	28.3	3.9
Co@N/Co-CNTs (CA: Co(acac) ₃ =10) ^a	1.26	90.33	4.8	3.62	44.5	10.2	37.8	7.4
Co@N/Co-CNTs (CA: Co(acac) ₃ =12) ^a	0.62	86.06	10.19	3.14	24.2	52.5	21.3	2.0
N-doped MWCNTs ^b	-	97.2	2.2	0.6	44.8	9.5	38.8	6.9

a) The mole ratio of CA to Co(acac)₃; b) the commercial N-doped MWCNTs.

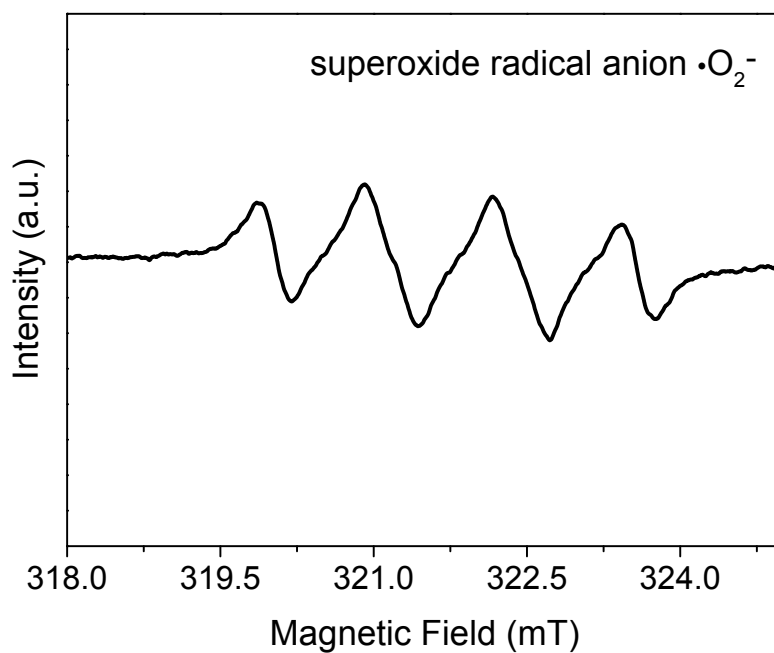


Fig. S14 DMPO spin-trapping EPR spectrum for Co@N/Co-CNTs in the aerobic oxidation of toluene, g : 2.0062; a_N : 13.28 G; a_H : 10.20 G.

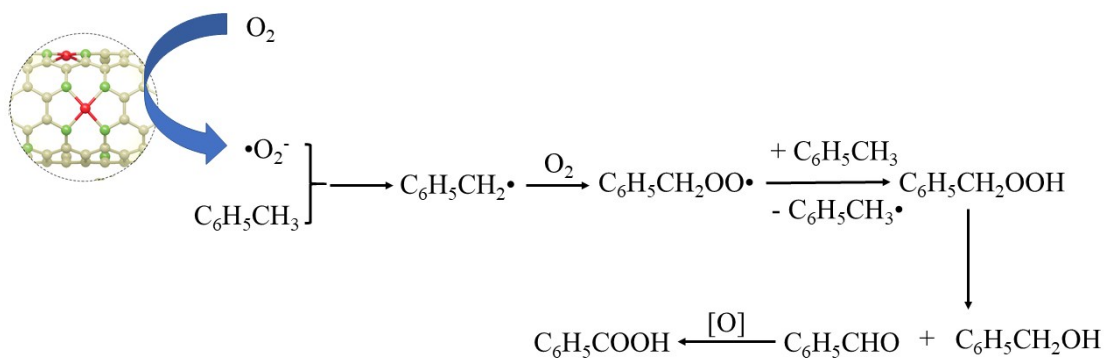


Fig. S15 The proposed toluene oxidation mechanism over Co@N/Co-CNTs.

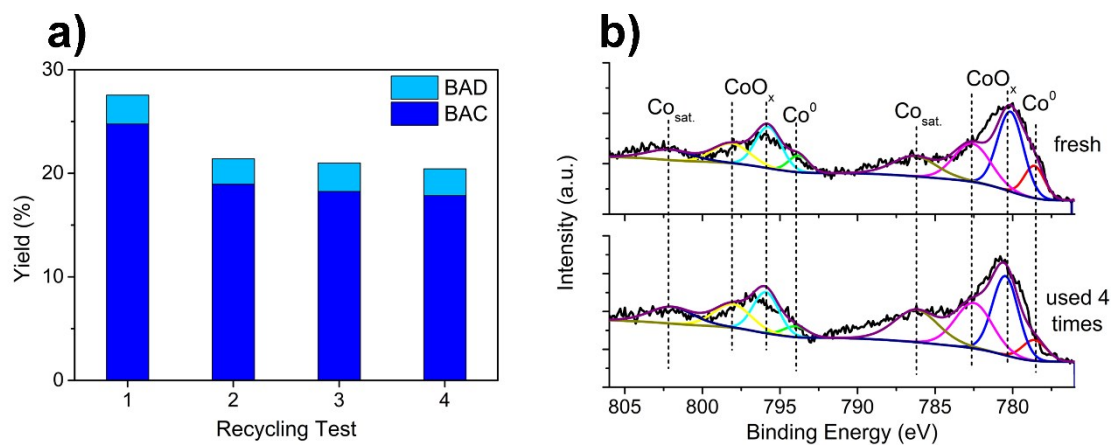


Fig. S16 a) The recycle experiment in the toluene oxidation with Co@N/Co-CNTs; b) the Co 2p XPS spectra of the fresh catalyst and reused for four times.

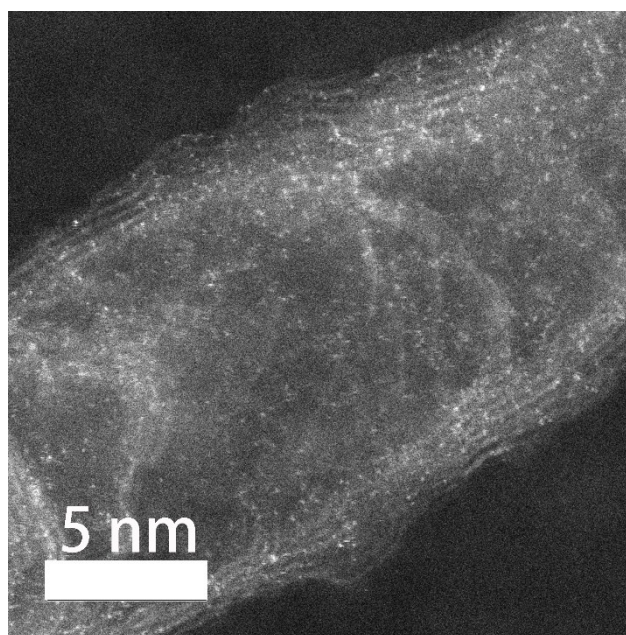


Fig. 17 HAADF-STEM image of the Co@N/Co-CNTs after cycling.

Table S5. Catalytic oxidation of xylene derivatives with the as-prepared Co@N/Co-CNTs.^a

Entry	Substrate	O ₂ (MPa)	T (°C) /t (h)	Con. (%) ^b	Sel (%) ^b		
					n-Tolualdehyde	n-Toluyalcohol	n-Toluic Acid
1	<i>o</i> -xylene	2	120/ 15	37.4	3.6	4.0	92.4
2	<i>m</i> -xylene	3	140/ 15	31.6	9.6	1.2	89.2
3	<i>p</i> -xylene	2	140/ 15	27.4	19.0	2.5	77.5
		3	120/ 15	33.0	14.9	2.1	83.0

a) Reaction conditions: xylenes (1.5 mL), catalyst (37.5 mg), O₂, heat/15 h; b) The conversions and selectivity were obtained by GC analysis using chlorobenzene as internal standard.

Table S6. Comparison of the catalytic performances for selective oxidation of toluene by various catalysts in the absence of radical additives.

Catalyst	Reaction conditions	Conv. (%)	BAC Sel. (%)	Ref.
Co@N/Co-CNTs	toluene 1.5 mL, catalyst 37.5 mg, O ₂ 3 MPa, 140 °C/24 h	33.5	91.6	This work
Au-Pd/C	toluene 20 mL, catalyst 0.4 g, 1.0 MPa O ₂ , 160 °C/7 h	4.8	10.3	[7]
Pt subnano-Catalysts (Pt SNCs)	toluene 2 mL, catalyst 10 mg, O ₂ 1 MPa, 160 °C/ 5 h	6.2 (TOF: 3238 atom ⁻¹ h ⁻¹)	61.8	[8]
Pt/ZrO ₂	toluene 10 mL, catalyst 0.2 g, O ₂ 101 kPa, flow rate of O ₂ /Air: 40 mL/min, 90 °C/ 3 h	37.2	70.4	[9]
Pd/ZrO ₂	toluene 10 mL, catalyst 0.2 g, flow of dioxygen, 100 °C/ 3.3 h	28.1	21.9	[10]
Pd-PMHS/TiO ₂	toluene 10.5 mL, catalyst 100 mg, O ₂ 2 MPa, 200 °C/ 8 h	10.4	9.7	[11]
Ag-Cu-BTC	toluene 10 mL, catalyst 0.1 g, O ₂ 1.0 MPa, 160 °C/ 4 h	13.0	1.1	[12]
Copper manganese oxides	toluene 50 mL, catalysts 1.0 g, O ₂ 1.0 MPa, 190 °C/ 2 h	21.6	73.7	[13]
MnO _x /SBA-15	toluene 25 mL, catalyst 100 mg, O ₂ 1.0 MPa, 180 °C/1 h	24.7	79.5	[14]
Layer-CoO _x /TiO ₂	toluene 27 mmol, catalyst 120 mg, O ₂ 1.7 MPa, 160 °C/ 16 h	9.9	13	[15]

3. References:

1. J. H. Xie, J. D. Kammert, N. Kaylor, J. W. Zheng, E. J. Choi, H. N. Pham, X. H. Sang, E. Stavitski, K. Attenkofer, R. R. Unocic, A. K. Datye, R. J. Davis, *ACS Catal.*, **2018**, *8*, 3875-3884.
2. a) J. Zhong, T. Xie, J. J. Deng, X. H. Sun, X. L. Pan, X. H. Bao, Z. Y. Wu, *Chem. Commun.*, **2011**, *47*, 8373-8375; b) T. Xie, Y. Zhao, J. Zhong, Z. Hu, X. H. Sun, *J. Appl. Phys.*, **2012**, *111*, 124318.
3. a) H. Zhang, X. Li, D. Zhang, L. Zhang, M. Kapilashrami, T. Sun, P. A. Glans, J. F. Zhu, J. Zhong, Z. Hu, J. H. Guo, X. H. Sun, *Carbon*, **2016**, *103*, 480-487; b) Y. Tong, P. Z. Chen, T. P. Zhou, K. Xu, W. S. Chu, C. Z. Wu, Y. Xie, *Angew. Chem. Int. Ed.*, **2017**, *56*, 7121-7125.
4. a) G. P. Mane, S. N. Talapaneni, K. S. Lakhi, H. Ilbeygi, U. Ravon, K. Al-Bahily, T. Mori, D. H. Park, A. Vinu, *Angew. Chem. Int. Ed.*, **2017**, *56*, 8481-8485; b) L. Zhang, F. X. Mao, L. R. Zheng, H. F. Wang, X. H. Yang, H. G. Yang, *ACS Catal.*, **2018**, *8*, 11035-11041.
5. X. X. Wang, D. A. Cullen, Y. T. Pan, S. Hwang, M. Y. Wang, Z. X. Feng, J. Y. Wang, M. H. Engelhard, H. G. Zhang, Y. H. He, Y. Y. Shao, D. Su, K. L. More, J. S. Spendelow, G. Wu, *Adv. Mater.*, **2018**, *30*, 1706758.
6. A. Tuxen, S. Carencio, M. Chintapalli, C. H. Chuang, C. Escudero, E. Pach, P. Jiang, F. Borondics, B. Beberwyck, A. P. Alivisatos, G. Thornton, W. F. Pong, J. H. Guo, R. Perez, F. Besenbacher, M. Salmeron, *J. Am. Chem. Soc.*, **2013**, *135*, 2273-2278.
7. L. Kesavan, R. Tiruvalam, M. H. Ab Rahim, M. I. bin Saiman, D. I. Enache, R. L. Jenkins, N. Dimitratos, J. A. Lopez-Sanchez, S. H. Taylor, D. W. Knight, C. J. Kiely, G. J. Hutchings, *Science*, **2011**, *331*, 195-199.
8. M. Huda, K. Minamisawa, T. Tsukamoto, M. Tanabe, K. Yamamoto, *Angew. Chem. Int. Ed.*, **2019**, *58*, 1002-1006.
9. M. Ilyas, M. Sadiq, *Catal. Lett.*, **2009**, *128*, 337-342.
10. M. Siddique, M. Saeed, M. Ilyas, H. Gulab, *Int. J. Chem. React. Eng.*, **2017**, *15*, 20160093.
11. B. Fu, X. Zhu, G. Xiao, *Appl. Catal. A: Gen.*, **2012**, *415-416*, 47-52.
12. Z. Sun, G. Li, Y. Zhang, H. Liu, X. Gao, *Catal. Commun.*, **2015**, *59*, 92-96.
13. X. Li, J. Xu, L. Zhou, F. Wang, J. Gao, C. Chen, J. Ning, H. Ma, *Catal. Lett.*, **2006**, *110*, 149-154
14. W. Zhong, S. R. Kirk, D. Yin, Y. Li, R. Zou, L. Mao, G. Zou, *Chem. Eng. J.*, **2015**, *280*, 737-747.
15. H. Wang, L. Wang, J. Zhang, C. Wang, Z. Liu, X. Gao, X. Meng, S. J. Yoo, J. G. Kim, W. Zhang, F. Xiao, *ChemSusChem*, **2018**, *11*, 3965-3974.